JOURNAL OF COMMUNICATION AND INFORMATION SYSTEMS, VOL. 33, NO.1, 2018.

138

Circularly Polarized Antenna Array with Sequential Rotation for Nanosatellites

Filipe G. Ferreira, Juner M. Vieira, Diego P. Fumagalli, Lucas S. Pereira and Marcos V. T. Heckler

Abstract—This paper presents the design and characterization of an aperture-coupled microstrip antenna array to be installed onto a nanosatellite. The proposed antenna array has been optimized to operate at 2.26 GHz (S-Band), which is the operating frequency of the downlink channel of the Brazilian System for Meteorological Data Acquisition. The electromagnetic analyses are done by using the HFSS electromagnetic simulator. For the design validation, prototypes of single elements and antenna array were manufactured. The comparison between simulations and measurements indicates good performance of the designed antennas.

Keywords—Antenna Array, Microstrip Antenna, Aperture-Coupled Antenna, Satellite Communications.

I. Introduction

In the last decades, the use of small satellites by the space industry has had an increase in popularity, especially in the military area, commercial business, universities, medium-sized companies and governmental research institutions. Compactness and mass reduction are some of the main features of small satellites that make them interesting candidates for low-cost space missions.

The satellites of the Brazilian Meteorological Data Collecting System (in Portuguese, *Sistema Brasileiro de Coleta de Dados* - SBCD) are in operation for more than fifteen years, which is beyond their expected lifetime. In order to replace these satellites, the National Institute for Space Research (INPE) started the CONASAT program, which aims at providing a new and much cheaper solution for using a constellation of nanosatellites.

The SBCD main purpose is to collect environmental data, such as rain volume, temperature, humidity, air pollution, ocean streams and environmental hazards, by deploying data collecting platforms in remote areas, such as in the Rain Forest or in the Atlantic Ocean. The SBCD must deliver this information to the Data Collection and Mission Control Center (in Portuguese, *Centro de Missão e Coleta de Dados* - CMCD) [2]. For this purpose, two independent communication channels are used: the uplink channel operates at UHF and the downlink at 2.26 GHz (S-Band).

Filipe G. Ferreira, Juner M. Vieira, Diego P. Fumagalli, Lucas S. Pereira and Marcos V. T. Heckler are with Electromagnetics, Microwaves and Antennas Laboratory (LEMA), Federal University of Pampa (UNIPAMPA), Alegrete, RS, Brazil. E-mail: marcos.heckler@unipampa.edu.br.

A critical aspect of the SBCD is the need of high reliability, so that the communication systems on-board the nanosatellites play an important role. Along with other important components of a satellite, the antenna must present high performance whilst exhibiting low weight and low volume. These are typical features of microtrip antenna technology, which, among other advantages, present design flexibility [3]. In order to minimize polarization mismatch, a circularly polarized antenna must be installed onto the nanosatellite. Antennas that fulfill such requirements have been reported in the literature. The authors in [4] proposed an active microstrip antenna array for satellite-based navigation. In [5], an antenna array in S-band for data downlink for nanosatellites is presented. In [6], the integration of two antenna arrays using thin substrates for simultaneous operation in S-Band and X-Band is discussed. A communication system at 2.4 GHz for LEO satellites including a low-cost 2x2 microstrip antenna array is described in [7]. The design of microstrip aperture-coupled antennas for microwave energy harvesting on a nanosatellite is analyzed in [8].

In this paper, the design and the performance of an antenna array for the downlink installed onto a nanosatellite is described. For this study, all electromagnetic analyses are done using commercial software and the performance is validated with measured results. The antenna array proposed has been designed to be compatible for installation onto a nanosatellite of the CONASAT Program. The following specifications apply for the antenna: operating frequency at 2.26 GHz, right-hand circular polarization (RHCP) with axial ratio lower than 3 dB, gain around 6 dBi, input impedance matched to 50 Ω, bandwidth of 50 MHz and maximum area of 20x20 cm^2 [2] .

The paper is organized in the following sections: the CONASAT program is briefly presented in section II; in section III, the details regarding the design of the single element with two linear orthogonal polarizations is discussed; sections IV and V present the design and construction of the prototypes. In section VI, the radiation characteristics of the microstrip antenna array will be presented; the final remarks are given in section VII.

II. Overview of the SBCD and the CONASAT Program

The ground section of the SBCD is composed of data collecting platforms (PCDs), which have been deployed over the whole Brazilian territory including the Atlantic coast, and the CMCD. Since some of the PCDs have been deployed in remote areas, such as in the Amazon region or even in the Atlantic, where no internet access is available, the nanosats

will serve as data relay for retransmitting the meteorological data collected by the PCDs to the CMCD [9], [10].

For transmitting the data from the ground to the satellites, the uplink channel works at 401 MHz (UHF) and a four-element microstrip antenna array with extended ground plane has been designed for this purpose [11]. For the downlink channel, another microstrip array is needed, since this link operates at 2.26 GHz (S-band). The transponder constitutes the nanosat payload, whose main functions are the translation of the received UHF signal into the transmit frequency and the delivering of the signal to the S-band antenna with appropriate power level. The CONASAT basic architecture and transponder block diagram are shown in Figure 1.
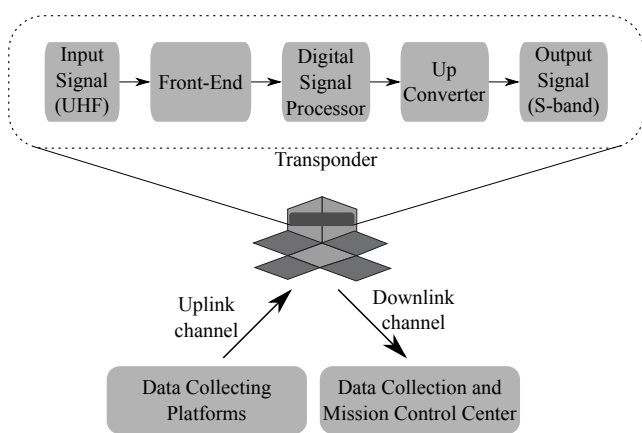
Fig. 1. Basic architecture of the CONASAT nanosatellite.

The size of the CONASAT nanosatellite is $8U$, according to the cubesat standards developed by the Space Flight Laboratory of Toronto University. This is equivalent to a cube with 20 cm of edge size and a maximum mass of 10 kg. Since energy in space is a critical issue, the nanosat will be equipped with four articulated flaps, so as to increase the area for installing solar panels [2]. The mechanical details of the nanosat are sketched in Figure 2.
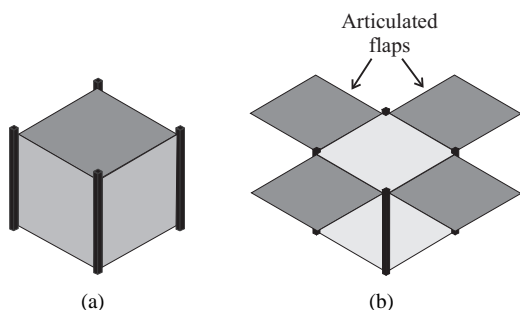
Fig. 2. Sketch of the nanosat structure: (a) with closed flaps (prior to launching); and (b) deployed configuration with open flaps.

The European policy for space debris mitigation (June 2004) foresees a maximum time for reentry, either natural or forced, as 25 years after the lifetime of the mission [2], [9]. In order to comply with this regulation, the nanosat must be deployed in an orbit at 600 km from the Earth surface.

III. MULTILAYER STRUCTURE OF THE SINGLE ELEMENT

In the proposed design, the microstrip antenna is fed by employing aperture coupling. By doing so, the feeding lines can be easily implemented in stripline technology, hence the pattern is not disturbed by spurious radiation. Moreover, this technique yields circular polarization with high purity [12], [13].

The proposed single element is composed of three dielectric layers. Figure 3 shows the cross-sectional view of the designed structure. The laminate used for the top and bottom layers is R04003C with $\varepsilon_r = 3.49$[1] and thickness of 1.524 mm. The intermediate laminate is RO4360G2 with $\varepsilon_r = 6.15$ and thickness of 0.610 mm. The prepeg Fast Rise 27 (FR27) was used to glue the three layers. The main characteristics of FR27 are: dielectric constant $\varepsilon_r = 2.75$ and thickness of 0.105 mm. The stripline is implemented using different laminates due to two main reasons: avoidance of parallel-plate TEM modes, which can be excited by the transitions existing in the power divider, and to improve power coupling between the feeding lines and the patches.
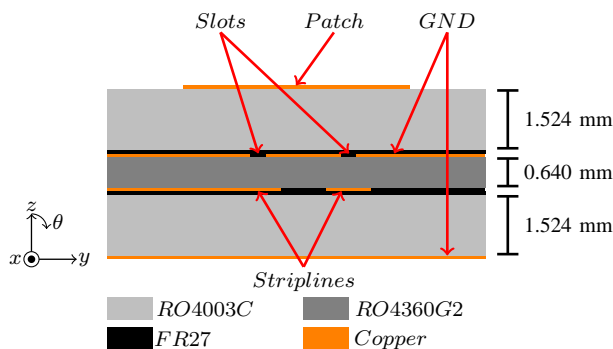
Fig. 3. Cross-sectional view of the designed antenna.

In standard aperture-coupled microstrip antennas, the patch length, feed line width and slot length are the physical parameters that govern the frequency of operation and impedance matching [3]. In the proposed design, a square patch is used due to the need of circular polarization. The coupling level is determined by the slot length: the larger the slot, the stronger the coupling between the patch and the feed line. However, an increase in the slot length results in larger power lost by excitation of surface waves [4], [14]. Therefore, the slots used in this design are small (non-resonating) and the impedance matching is ensured by employing the double-stub technique [15]. The patch edge sizes are set so as to tune the antenna to the maximum possible gain in the operating frequency. Once the lengths for patch and slots have been defined, impedance matching is achieved only by varying the lengths of both stubs.

Circular polarization can be obtained by exciting two orthogonal modes (TM_{10}^z and TM_{01}^z) in the patch. These modes are excited by using two slots and by introducing a $\pm90°$ phase shift between them, whereby the $\pm$ sign stands for the sense of rotation of the electric field is to the right (right-hand circular polarization) or to the left (left-hand circular polarization).

---

[1]This value has been obtained experimentally prior to this antenna design.

IV. Preliminary Antenna Design

The antenna design procedure started with the impedance matching for the antenna with two feeding lines. Since circular polarization is required, Ports 1 and 2 were fed with signals presenting $90°$ phase shift between them, so as to generate a radiation pattern with RHCP as the main polarization. The geometry of the element is shown in Figure 4 [1]. As commented before, impedance matching is done mostly by adjusting the lengths of the stubs. The distance between the slots and the patch center governs the coupling between the two feeding lines and has direct influence on the axial ratio (AR): the larger the coupling, the poorer the axial ratio. After the optimization process, the physical dimensions obtained are summarized in Table I.
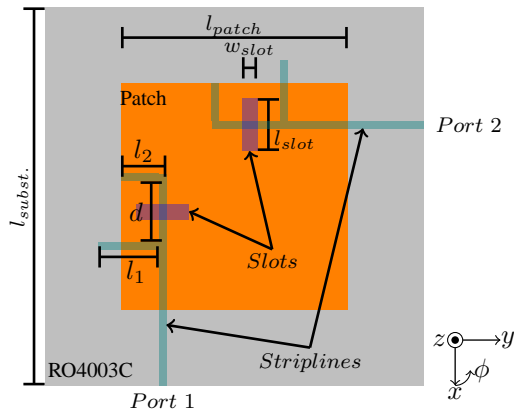
Fig. 4. Schematic top view of the designed antenna.

TABLE I
DIMENSIONS OF THE DESIGNED ANTENNA.

Parameter	Dimension (in mm)
Substrate size ($l_{subst.}$)	80.80
Patch size (l_{patch})	34.64
Distance between stubs (d)	10.66
Length stub 1 (l_1)	11.20
Length stub 2 (l_2)	6.60
Length slot (l_{slot})	9.00
Width slot (w_{slot})	1.80
Slot displacement from the center of the patch	9.40
Width feeding stripline	0.66

The simulated AR as a function of the frequency and as a function of the elevation angle (θ) is shown in Figures 5 and 6, respectively. At 2.26 GHz, the axial ratio is below 1.2 dB in the boresight direction. By considering values of AR below 3 dB, the field of view with acceptable AR is $130°$ at the center operation frequency.

In order to validate the design, a prototype was manufactured and a photo is presented in Figure 7. The comparison between simulated (S) and measured (M) S-parameters is shown in Figure 8. High isolation between the ports was obtained. Frequency shifts of 14 MHz for the S_{11} parameter and 21 MHz for S_{22} were verified.

To investigate these discrepancies, a parametric study of the dielectric constant of the laminate RO4003C was done by
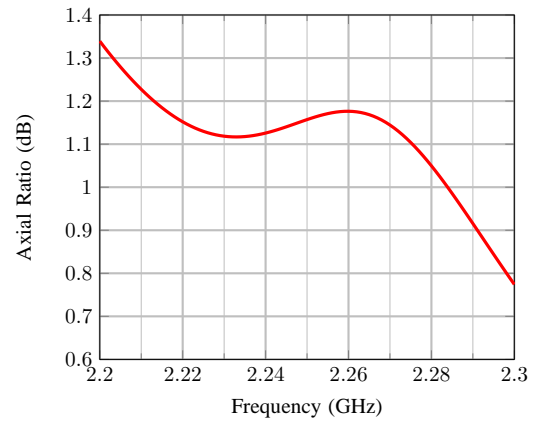
Fig. 5. Simulated axial ratio as a function of the frequency for the designed antenna in the boresight direction ($\theta = 0°$).
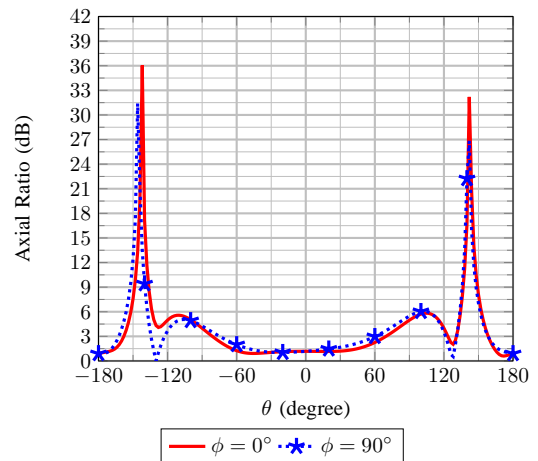
Fig. 6. Simulated axial ratio as a function of the elevation angle for the designed antenna, at 2.26 GHz.
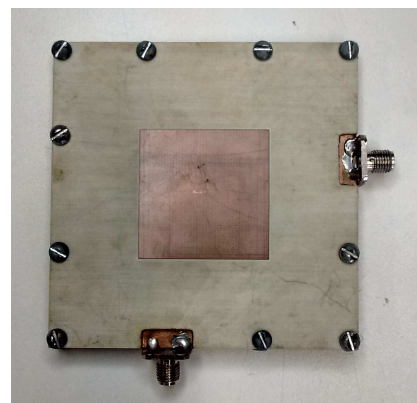
Fig. 7. Top view of the prototype.

keeping the designed antenna dimensions. In this new simulation, the use of $\varepsilon_r = 3.43$ instead of 3.49 for the RO4003C laminate resulted in good agreement with the measured curves, as demonstrated in Figure 9. The value $\varepsilon_r = 3.43$ has been used for the design hereafter.

Radiation pattern measurements have been carried out using a spherical near-field scanner (NFS). An external $90°$-hybrid
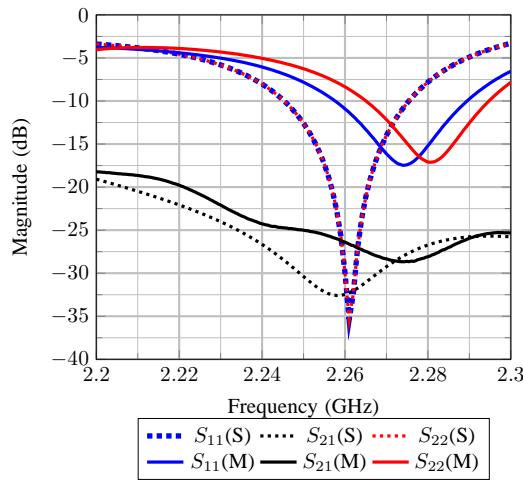
Fig. 8. Comparison between simulated (S) and measured (M) S-parameters for the designed antenna.
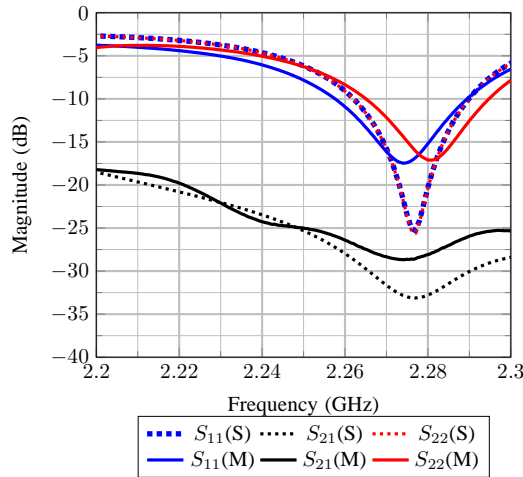
Fig. 9. Comparison between simulated (using $\varepsilon_r = 3.43$) and measured S-parameters for the designed antenna.

was connected to the antenna terminals, so as to produce the necessary $90°$ phase shift needed for circular polarization. A photo showing the measurement setup is presented in Figure 10. Figure 11 presents the comparison between simulated and measured normalized radiation patterns. The simulated maximum gain obtained for this antenna is 6 dBi and the half-power beamwidth (HPBW) obtained is $84°$. One can observe that very good agreement for the principal polarization was obtained, and high cross-polarization decoupling in the boresight, which is larger than 25 dB, is verified.

V. ANTENNA WITH AN INTEGRATED 90° HYBRID COUPLER

In order to increase antenna compactness, a $90°$ hybrid was integrated into the multilayer structure. The hybrid was designed and the resulting physical dimensions are listed in Table II according to the convention sketched in Figure 12.

Electromagnetic simulations were done after the integration of the hybrid into the antenna feeding system. The simulated S-parameters are presented in Figure 13. The simulated AR as

(a)   (b)
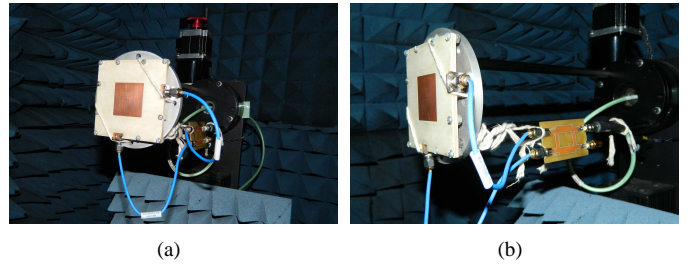
Fig. 10. Measurement setup of the antenna connected to an external $90°$ hybrid.

(a) Plane $\phi = 0°$.

(b) Plane $\phi = 90°$.
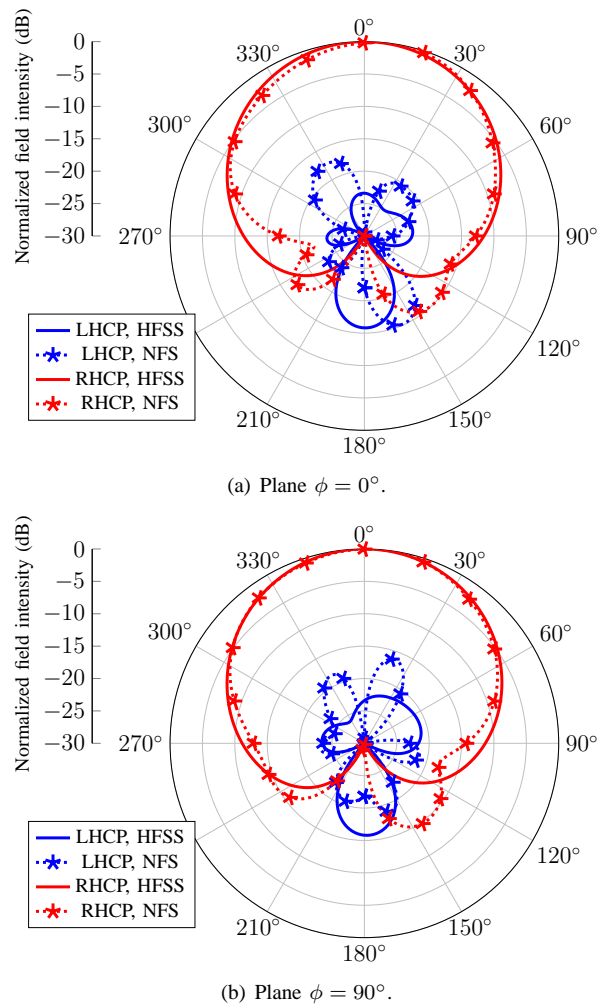
Fig. 11. Comparison between simulated and measured radiation patterns at 2.26 GHz for different azimuth (ϕ) planes.

TABLE II
DIMENSIONS OF THE 90° HYBRID.

Parameter	Dimension (in mm)
$L_{50\Omega}$	14.62
$W_{50\Omega}$	0.66
$L_{35.35\Omega}$	14.54
$W_{35.35\Omega}$	1.30

a function of the frequency and of the elevation angle (θ) are shown in Figures 14 and 15, respectively. The resulting AR is
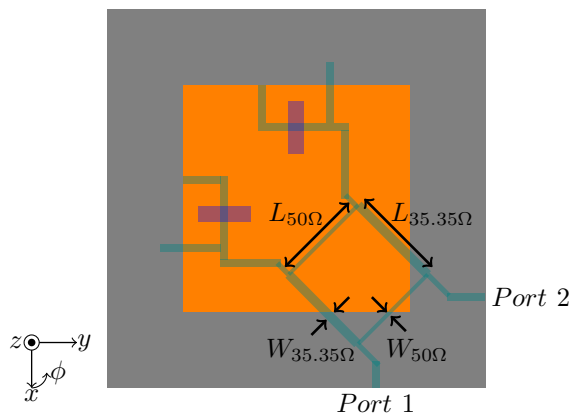
Fig. 12. Schematic top view of the designed antenna with an integrated 90° hybrid.

below 3 dB for an angular region of approximately 130°. The simulated gain pattern was plotted and is shown in Figure 16. Large cross-polarization decoupling can be observed and the maximum simulated gain obtained was 5.97 dBi.
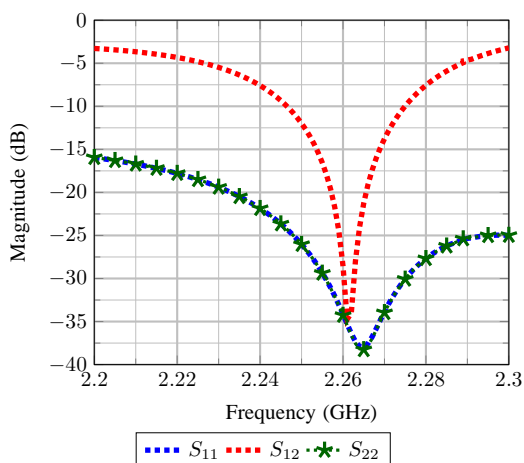
Fig. 13. Variation of the S-parameters with the frequency for the antenna with an integrated 90° hybrid.
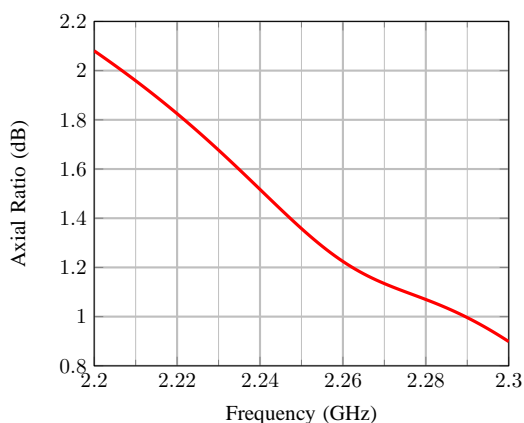
Fig. 14. Simulated axial ratio as a function of the frequency for the antenna with an integrated 90° hybrid in the boresight direction ($\theta = 0°$) .
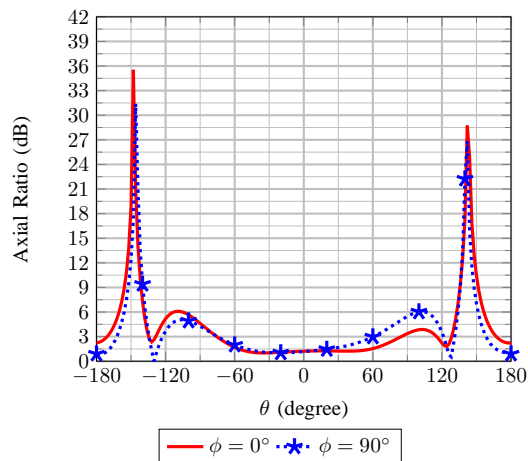
Fig. 15. Simulated axial ratio as a function of the elevation angle for the antenna with an integrated 90° hybrid, at 2.26 GHz.
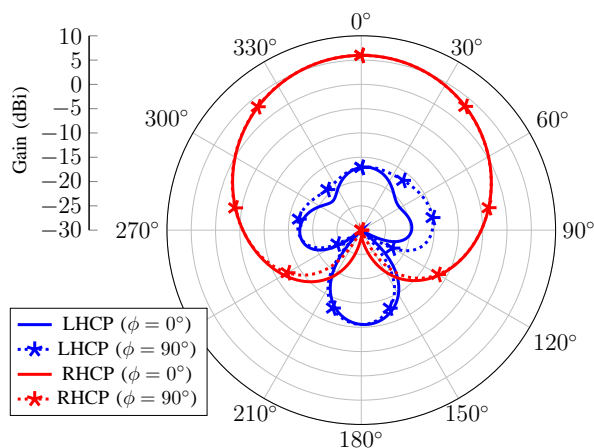
Fig. 16. Simulated gain pattern at 2.26 GHz for different azimuth (ϕ) planes.

VI. ANTENNA ARRAY DESIGN

Due to space constraints, the designed antenna can be used to compose an array with a maximum size of 2x2 elements. This would allow obtaining larger gain than by using a single radiator, hence reducing the transmitting power needed to establish the downlink.

The first design approach considered was the integration of the designed antenna into a 2x2 array according to the geometry shown in Figure 17. The excitation ports for the electromagnetic simulations and the SMD resistors used to terminate the isolated ports of the 90° hybrids are indicated by dashed blue and red circles, respectively. In order to maximize the gain, the inter-element distance was set to 80.8 mm, which corresponds to 0.67 λ_0, where λ_0 is the wavelength in free space at 2.26 GHz.

The RHCP and LHCP gain patterns for different planes are shown in Figure 18. A decrease in terms of cross polarization discrimination (XPD) can be observed when compared with the radiation pattern of the single element shown in Figure 16. The magnitude of XPD obtained was 15 dB, which corresponds to an axial ratio of roughly 3 dB.
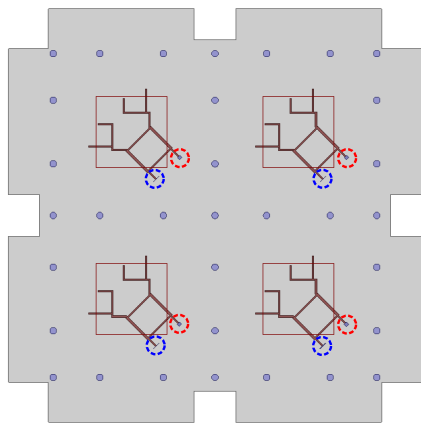
Fig. 17.   Schematic top view of a classical 2x2 planar antenna array (elements with the same orientation).
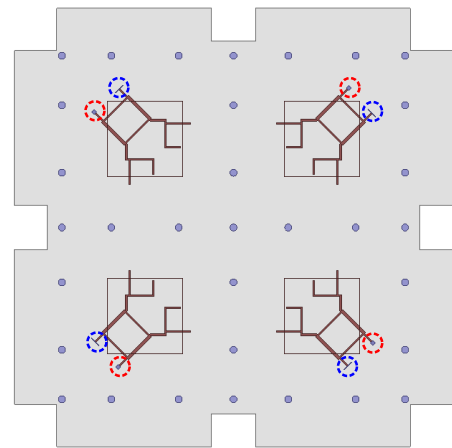
Fig. 19.   Schematic top view of the antenna array with sequential rotation of elements.
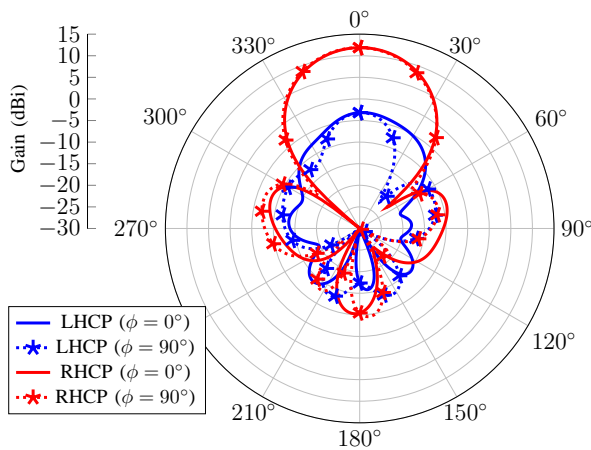
Fig. 18.   Simulated gain pattern at 2.26 GHz for different azimuth (ϕ) planes for the classical 2x2 antenna array.
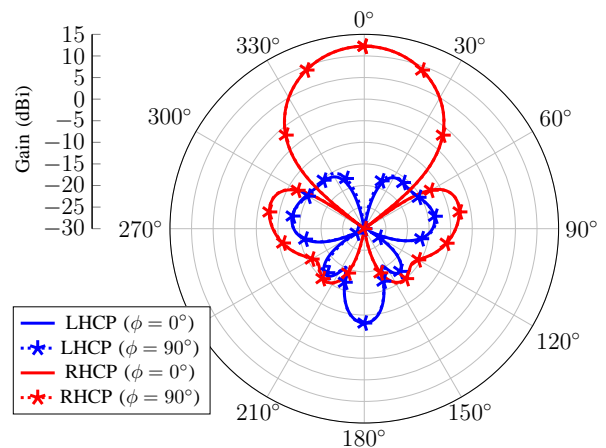
Fig. 20.   Simulated gain pattern at 2.26 GHz for different azimuth (ϕ) planes for the array with sequential rotation of elements.

In order to improve the performance in terms of polarization purity, the second design approach considered sequential rotation of the array elements. In this technique, a physical rotation of the elements along with a proper phase shift between the excitation currents must be done. This approach yields wideband CP behavior and high polarization purity [16], [17]. The main drawback of this technique is the need of a more complex feeding network to provide the necessary phase shifts between the array elements. The resulting array geometry is depicted in Figure 19.

The results in terms of co-polarization and cross-polarization are presented in Figure 20. The level of XPD obtained by simulation was larger than 40 dB. Consequently, an improvement terms of axial ratio (AR) was obtained. The comparison between the two design approaches is detailed in Figure 21. The improvement in the polarization purity becomes evident by the use of sequential rotation of the array elements. Fig. 22 shows the variation of the axial ratio as a function of the elevation angle (θ) at 2.26 GHz.

A prototype of the 2x2 antenna array was designed and fabricated by integrating the feeding network to provide the four antennas with progressive phase shift of 90°. The
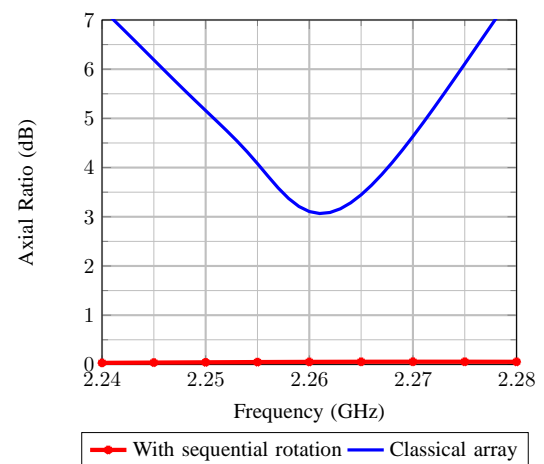
Fig. 21.   Comparison between simulated axial ratio of antenna array considering the two design approaches in the boresight direction ($\theta = 0°$).

fabricated antenna is shown in Figure 23. The locations of the SMD resistors are indicated by blue dashed circles and the input connector is marked in red. The total size of the array is 200 mm x 200 mm, hence fulfilling the maximum
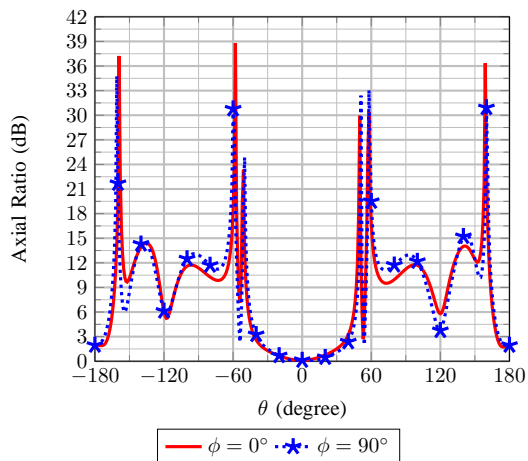
Fig. 22. Simulated axial ratio as a function of the elevation angle at 2.26 GHz for the antenna array with sequential rotation of elements.
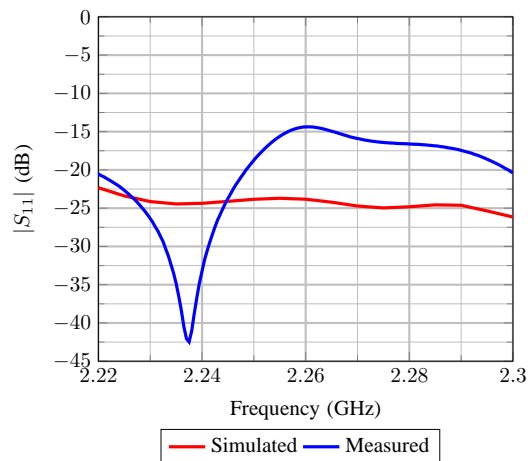
Fig. 24. Comparison between measured and simulated reflection coefficient for the fabricated 2x2 antenna array.

area specification. A comparison between computational and measured results in terms of reflection coefficient is shown in Figure 24. The main reason for the discrepancies is attributed to slight misalignment between the laminates after the gluing process. Despite the discrepancy between the curves, all the experimental values are located below -10 dB, so that the specification for maximum reflection coefficient has been fulfilled too.

Fig. 23. Photos of the fabricated prototype: (a) feeding system in stripline technology prior to the final assembly; (b) patches in 2x2 configuration.

The radiation patterns simulated and measured have been undertaken by installing the antenna array onto the nanosat engineering model in deployed configuration (i.e. with open flaps). The UHF receiving antenna array described in [11] has been also installed onto the nano-sat mock-up to assess the deterioration of performance due to the mutual coupling. A photo of the nanosat is shown in Figure 25. A comparison between simulated and measured results for the normalized radiation patterns with the antenna array mounted onto the nanosat engineering model is presented in Figure 26. Good agreement in terms of co-polarization can be observed. The level of the measured cross-polarization decoupling in the boresight is 18 dB, which is equivalent to an AR of roughly 2.2 dB, so that the specification for polarization purity has been also fulfilled.

Fig. 25. Nanosat engineering model with on-board S-band (in the center) and UHF arrays.
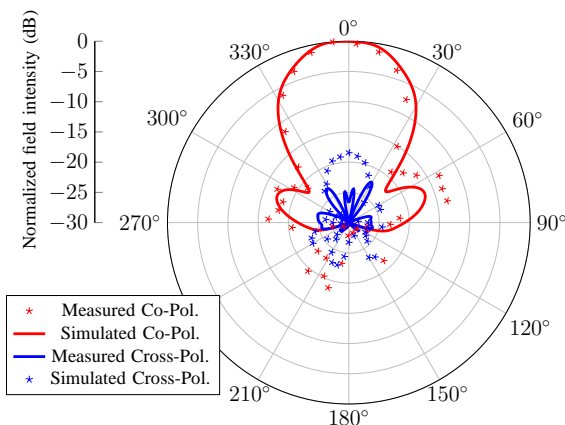
Fig. 26. Comparison between measured and simulated pattern at 2.26 GHz.

VII. Conclusions

In this paper, the design of a circularly polarized microstrip antenna operating in the S-band for nanosatellite has been described. The design started with impedance matching between the patch and two feeding lines. This model exhibits

two orthogonal linear polarizations and was manufactured and measured. The simulated gain of the single element operating at 2.26 GHz was 6 dBi. Although the measured S-parameters presented a frequency deviation, which has been attributed to the dielectric constant value used in the simulations, the measured radiation pattern showed good agreement with the simulations and large cross-polarization decoupling. The second design step was the integration of a 90° hybrid into the antenna structure. In terms of axial ratio and gain, the results obtained were similar to those obtained with a linearly polarized geometry with an external 90° hybrid. A 2x2 array has been designed based on the developed single element. The performance of this array has been validated by measured results, which demonstrated that all the electrical specifications have been fulfilled with a compact antenna.

ACKNOWLEDGEMENTS

REFERENCES

[1] F. Ferreira, J. M. Vieira, D. Fumagalli, L. S. Pereira, and M. V. T. Heckler, "Circularly Polarized Aperture-Coupled Microstrip Antenna for Nano-Satellites," in *XXXV Simpósio Brasileiro de Telecomunicações e Processamento de Sinais (SBrT 2017)*, São Pedro, Brazil, Sep. 2017, pp. 57–61.

[2] INPE, *Documento de Descrição da Missão (DDM)*, Centro Regional do Nordeste - Instituto Nacional de Pesquisas Espaciais (CRN/INPE), Natal-RN, 2011. [Online]. Available: http://www.crn2.inpe.br/conasat1/docprojeto.php

[3] C. A. Balanis, *Antenna Theory: Analysis and Design*. John Wiley & Sons, 2005, vol. 1.

[4] M. V. T. Heckler, W. Elmarissi, L. A. Greda, M. Cuntz, and A. Dreher, "Narrow-Band Microstrip Antenna Array for a Robust Receiver for Navigation Applications," in *Antennas and Propagation, 2009. EuCAP 2009. 3rd European Conference on*. IEEE, 2009, pp. 1206–1210.

[5] T. Sreeja, A. Arun, and J. Jaya Kumari, "An S-Band Micro-strip Patch Array Antenna for Nano-Satellite Applications," in *Green Technologies (ICGT), 2012 International Conference on*. IEEE, 2012, pp. 325–328, DOI: 10.1109/ICGT.2012.6477994.

[6] S. H. Hsu, Y. J. Ren, and K. Chang, "A Dual-Polarized Planar-Array Antenna for S-Band and X-Band Airborne Applications," *Antennas and Propagation Magazine, IEEE*, vol. 51, no. 4, pp. 70–78, 2009, DOI: 10.1109/MAP.2009.5338685.

[7] O. Ceylan, Y. Kurt, F. A. Tunc, H. B. Yagci, and A. R. Aslan, "Low Cost S Band Communication System Design for Nano Satellites," in *Proceedings of 5th International Conference on Recent Advances in Space Technologies - RAST2011*, June 2011, pp. 767–770, DOI: 10.1109/RAST.2011.5966945.

[8] C. A. M. Bergsrud and S. Noghanian, "Microstrip Aperture-Coupled Antenna Design for in Space Power Reception Experiment Using Nano Sized Satellite," in *2015 USNC-URSI Radio Science Meeting (Joint with AP-S Symposium)*, July 2015, pp. 25–25, DOI: 10.1109/USNC-URSI.2015.7303309.

[9] M. J. M. de Carvalho, J. S. dos Santos Lima, L. dos Santos Jotha, and P. S. de Aquino, "CONASAT - Constelação de Nano Satélites para Coleta de Dados Ambientais," *XVI Simpósio Brasileiro de Sensoriamento Remoto*, pp. 9108–9115, 2013.

[10] W. Yamaguti, V. Orlando, and S. Pereira, "Sistema Brasileiro de Coleta de Dados Ambientais: Status e Planos Futuros," *XIV Simpósio Brasileiro de Sensoriamento Remoto*, vol. 14, pp. 1633–1640, 2009.

[11] J. M. Vieira, M. P. Magalhães, M. V. T. Heckler, J. C. M. Mota, and A. S. Sombra, "Development of an UHF 2 x 2 Microstrip Antenna Array for Nano-Satellites," *Journal of Communication and Information Systems*, vol. 31, no. 1, 2016, DOI: 10.14209/jcis.2016.13.

[12] D. M. Pozar, "Microstrip Antenna Aperture-Coupled to a Microstripline," *Electronics Letters*, vol. 21, no. 2, pp. 49–50, January 1985, DOI: 10.1049/el:19850034.

[13] K. M. Luk, T. M. Au, K. F. Tong, and K. F. LEE, *Aperture-Coupled Multilayer Microstrip Antennas*. John Wiley & Sons, ch. 2, pp. 71 – 122.

[14] M. P. David, "A Review of Aperture Coupled Microstrip Antennas: History, Operation, Development, and Applications by," 1996.

[15] D. M. Pozar, *Microwave Engineering*. John Wiley & Sons, 2009.

[16] R. Garg, P. Bhartia, I. Bahl, and A. Ittipiboon, *Microstrip Antenna Design Handbook*. Artech house, 2001.

[17] P. S. Hall, "Application of Sequential Feeding to Wide Bandwidth, Circularly Polarised Microstrip Patch Arrays," *IEE Proceedings H - Microwaves, Antennas and Propagation*, vol. 136, no. 5, pp. 390–398, Oct 1989.

Filipe Guterres Ferreira was born in Alegrete, Brazil, in 1994. He received the BSc degree in Telecommunications Engineering from Universidade Federal do Pampa (UNIPAMPA) in 2016, Alegrete, Brazil. His current research interests are the design of antennas and passive microwave devices.

Juner Menezes Vieira was born in Alegrete, Brazil, in 1984. He received the BSc degree in Telecommunications Engineering from Universidade Federal do Pampa (UNIPAMPA) in 2017, Alegrete, Brazil. Currently is a master student at UNIPAMPA. He is member of the Electromagnetics, Microwaves and Antennas Laboratory (LEMA). His current research interests are the design of microstrip antennas arrays for data communications and the development of antennas for telemetry and telecommand, both applied in nanosatellites.

Diego Pereira Fumagalli was born in Julio de Castilhos, Brazil, in 1986. He received the technical degree in Telecommunications (2012) from Escola de Educação Profissional e Técnica - CIETEC, Brasil. Currently is graduation student of Computer Science and since 2013 he has been workin as a member of the technical staff at UNIPAMPA in the Electromagnetics, Microwaves and Antennas Laboratory (LEMA).

Lucas Santos Pereira was born in São Luiz Gonzaga, Brazil, in 1990. He received the BSc. degree (2013) in Electrical Engineering (Emphasis in Electrical Power Systems) and the MSc. Degree in Electrical Engineering in 2015 (Emphasis in Energy Systems), both from Universidade Federal do Pampa, Alegrete, Brazil. He has been working as a teaching assistant at UNIPAMPA since 2013 in the field of Telecommunications Engineering. His current research interest is the design of dual-band microstrip antennas.

Marcos Vinício Thomas Heckler was born in Rio Grande, Brazil, in 1978. He received the BSc. Degree in Electrical Engineering (Emphasis in Electronics) in 2001 from Universidade Federal de Santa Maria – UFSM, Brazil, the MSc. Degree in Electronic Engineering (Microwaves and Opto-electronics) in 2003 from Instituto Tecnológico de Aeronáutica – ITA, Brazil, and the Dr.–Ing. Degree in Electrical Engineering in 2010 from Technische Universität München – TUM, Germany. From April to August 2003 he worked as a Research Assistant with the Antennas and Propagation Laboratory at ITA, Brazil. From October 2003 to June 2010 he worked as a Research Associate towards his PhD with the Antenna Group, Institute of Communications and Navigation, German Aerospace Center – DLR. He is currently a Professor at UNIPAMPA, in Alegrete, Brazil. His current research interests are the design of microstrip antennas and arrays, and the development of numerical techniques for microstrip antennas. Prof. Heckler is the Head of the Electromagnetics, Microwaves and Antennas Laboratory (LEMA) at UNIPAMPA.